Hierarchical complexity of the neonatal brain

Manuel Blesa[a], Paola Galdi[a], Simon R. Cox[e], David Q. Stoye[a], Gemma Sullivan[a], Gillian J. Lamb[a], Alan J. Quigley[d], Michael J. Thrippleton[e, f], Javier Escudero[f], Mark E. Bastin[e], Catherine Sudlow[b], Keith M. Smith[b,c,1] & James P. Boardman [a, e,1].
[a]MRC Centre for Reproductive Health, University of Edinburgh, Edinburgh EH16 4TJ, UK
[b]Usher Institute, University of Edinburgh, Edinburgh EH16 4UX, UK
[c]Health Data Research UK, London NW1 2BE, UK
[d]Department of Radiology, Royal Hospital for Sick Children, Edinburgh EH9 1LF, UK
[e]Centre for Clinical Brain Sciences, University of Edinburgh, Edinburgh EH16 4SB, UK
[f]Edinburgh Imaging, University of Edinburgh, Edinburgh EH16 4SB, UK
[1]Equal contribution.

Introduction:

Preterm birth is associated with long term cognitive deficits and alterations to structural connectivity of developing brain networks. Global network characteristics modelled topological properties of brain regions and the connections between them reveal architectures that are shared across the life course. These include small-worldness, clustering coefficient or rich-club coefficient[1-3]. In recent work, it was shown that a rich diversity of connectivity patterns within hierarchically equivalent nodes (hierarchical complexity, HC)[4], is a strong signature of the adult human connectome and not a general property of real-world networks like several of the other standard global network metrics[5]. We aimed to determine whether the newborn brain resembles the adult in terms of HC, if so, whether HC is altered in association with early exposure to extrauterine life caused by preterm birth.

Methods:

Neonatal dataset: 136 neonates (77 preterm and 59 term) underwent MRI at term equivalent age at the Edinburgh Imaging Facility Royal Infirmary of Edinburgh. A Siemens MAGNETOM Prisma 3 T MRI clinical scanner (Siemens Healthcare Erlangen, Germany) and 16-channel phased-array paediatric head coil were used to acquire: 3D T2-weighted SPACE (T2w) (voxel size = 1mm isotropic) and axial dMRI with volumes/b = 3/200, 6/500, 64/750 and 64/2500 s/mm^2 and 16 non-weighted images (2mm isotropic).

Adult dataset: The HCP test-retest dataset consisting of T1-weighted and DW-MRI data from 45 healthy subjects. The data consist of three shells with b = 1,000, 2,000 and 3,000 s/mm^2 in 90 DW volumes and six non-weighted images per shell (1.25 mm isotropic).

Processing: The neonatal dMRI volumes were denoised[6]; the eddy current, head movement and EPI geometric distortions were corrected[7-9], and bias field inhomogeneity correction was applied[10]. The T2w images were processed using the minimal processing pipeline of the dHCP[11]. For parcellation, ten manually labelled subjects of the M-CRIB atlas[12] were registered to the bias field corrected T2w using affine and SyN[13], and then the registered labels of the ten atlases were merged using joint label fusion[14] resulting in 84 ROIs. The HCP dataset was already preprocessed, with the Desikan-Killany parcellation[15, 16].

Tractography was performed using CSD with multi-tissue response function, using ACT and SIFT2[17-21]. The resulting matrices were then thresholded to a density of 0.3 and binarized.

Hierarchical complexity: Let $G = (V, E)$ be a graph with nodes $V = \{1, \dots, n\}$ and links $E =$

$\{(i,j): i,j \in V)\}$, and let $K = \{k_1, \dots, k_n\}$ be the set of degrees of G, where k_i is the number edges adjacent to node i. Further, let K_p be the set of nodes of degree p. For neighbourhood degree sequence $s_i^p\{s_i^p(1), \dots, s_i^p(p)\}$ of node i of degree p, the HC is:

$$R = \frac{1}{D} \sum_{k_p, |k_p|>1} \frac{1}{p(|k_p| - 1)} \left(\sum_{j-1}^{p} \left(\sum_{i \epsilon k_p} (s_i^p(j) - \mu^p(j))^2\right)\right)$$

where D is the number of distinct degrees in the network and $\mu^p(j)$ is the mean of the jth entries of all p length neighbourhood degree sequences[22].

Tier analysis: A more refined analysis of HC was performed through different degree strengths in the network. The tiers were chosen based on peaks of the group-aggregated degree distributions, 4 tiers were chosen in each population (1-4) and were combined then into 3 Tiers (A-C) to be able to compare neonates and adults. Once tiers were defined, we implemented tier-based analysis comparing Tiers 1-4 between term and preterm born and A-C between neonates and adults.

Statistical analysis: To control for the differences in degree distribution between individual connectomes and the different populations (term and preterm born and adult), we used configuration models[23]. Wilcoxon rank sum tests were carried out to assess the significance of the differences of distributions of network index values between the structural connectomes and configuration models. FDR threshold was 0.0264. The effect sizes were also computed with Cohen's d.

Results:

Figure 1 shows the group-aggregated degree distributions.

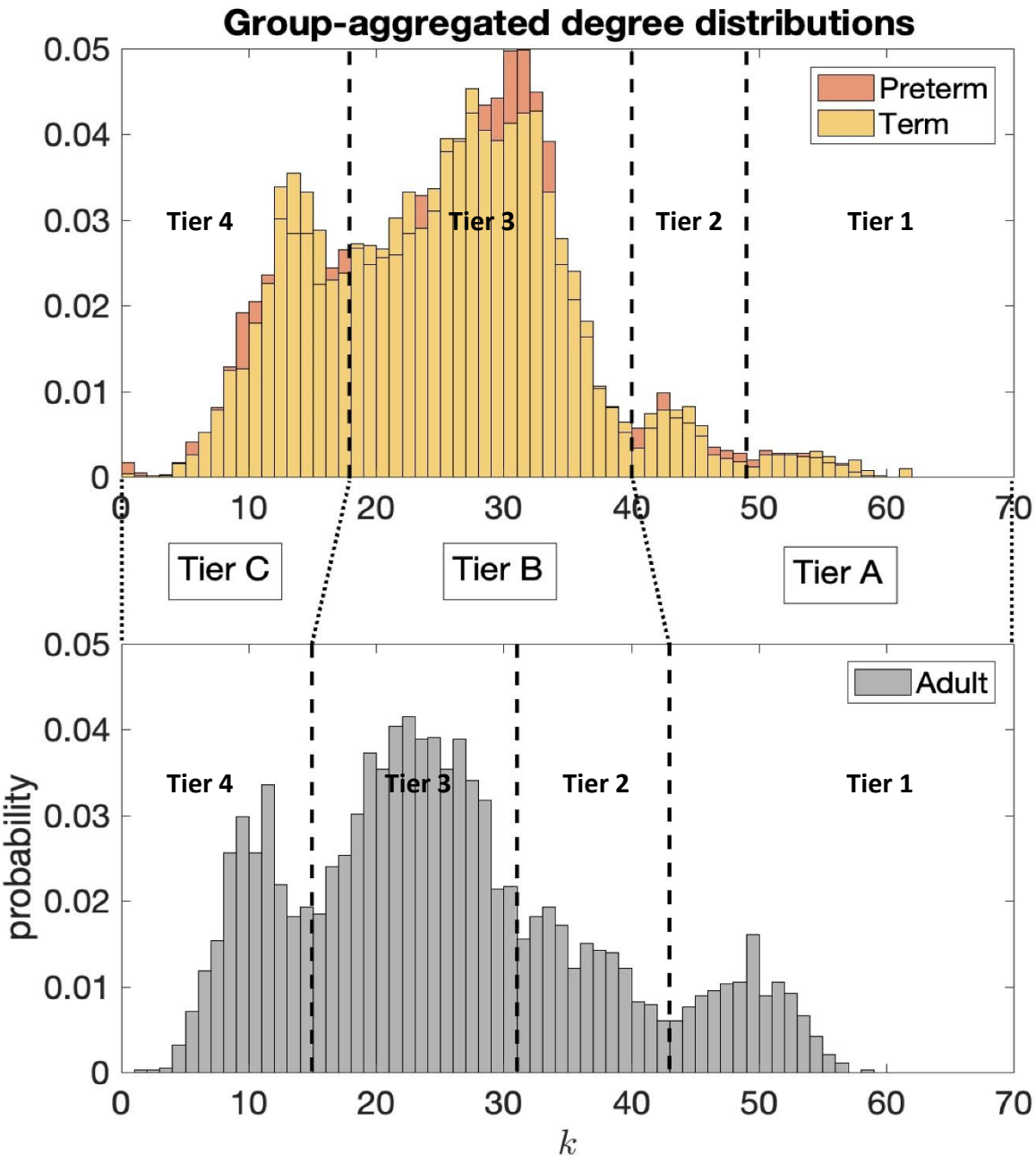

Figure 1: Aggregated degree distributions of neonatal groups, top, and the adult group, bottom. Four distinct peaks are noted in the degree distributions of neonatal connectomes and corresponding peaks are also seen in the adult connectomes. These are taken as the natural tiers and black lines indicating the minima between peaks are taken as the thresholds between tiers. Greater consistency between neonates and adults is found by consolidating the tiers as indicated by Tier A, B and C.

HC was significantly larger in term-born neonates than preterm-born neonates (p = 0.0148, d = 0.3946). Tier 3 showed a corresponding significant difference in HC with a stronger effect size (p = 2.63×10^{-4}, d = 0.6230), while no difference was evident in any other tier. Global HC of adults was larger than term born neonates (p = 2.63×10^{-11}, d = 1.2859) (Fig 2). The findings were confirmed in comparisons with configuration models

with term-born connectomes having significantly larger HC than their configuration models, an effect which was not seen in preterm infants (Fig 3).

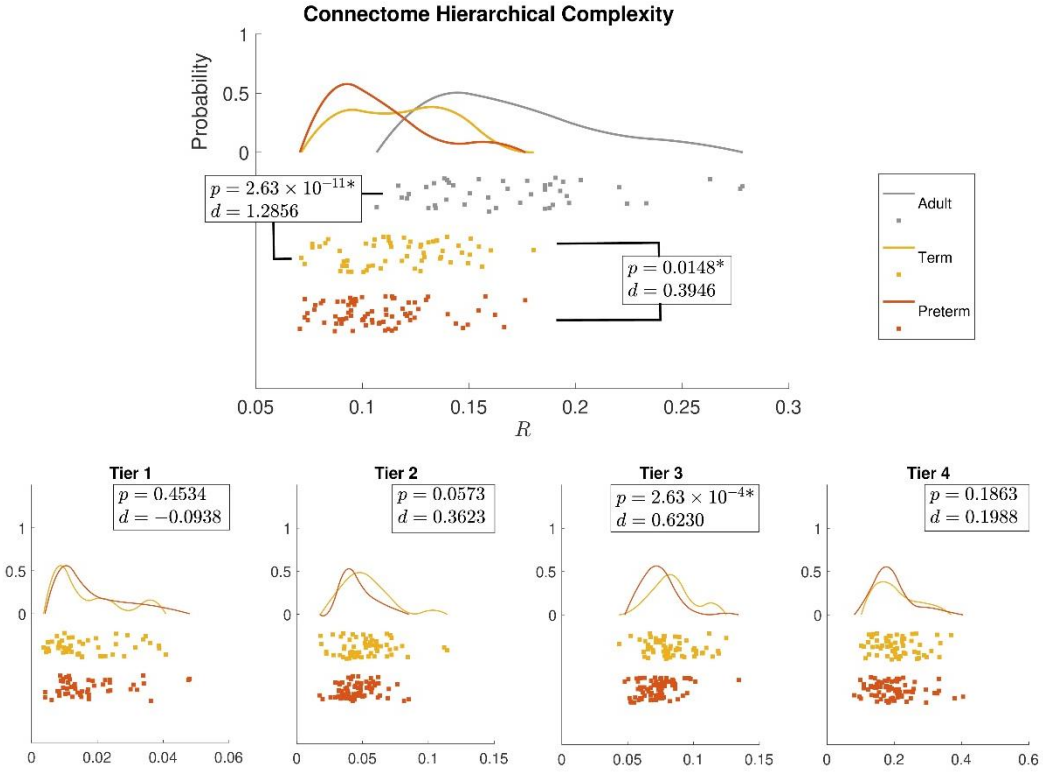

Figure 2: Distribution of the global HC for the three populations as rain cloud plots (top) and HC of the four tiers in neonatal populations (bottom). Wilcoxon rank sum p-values and Cohen's d values are shown for preterm vs term (all) and term vs adult (top).

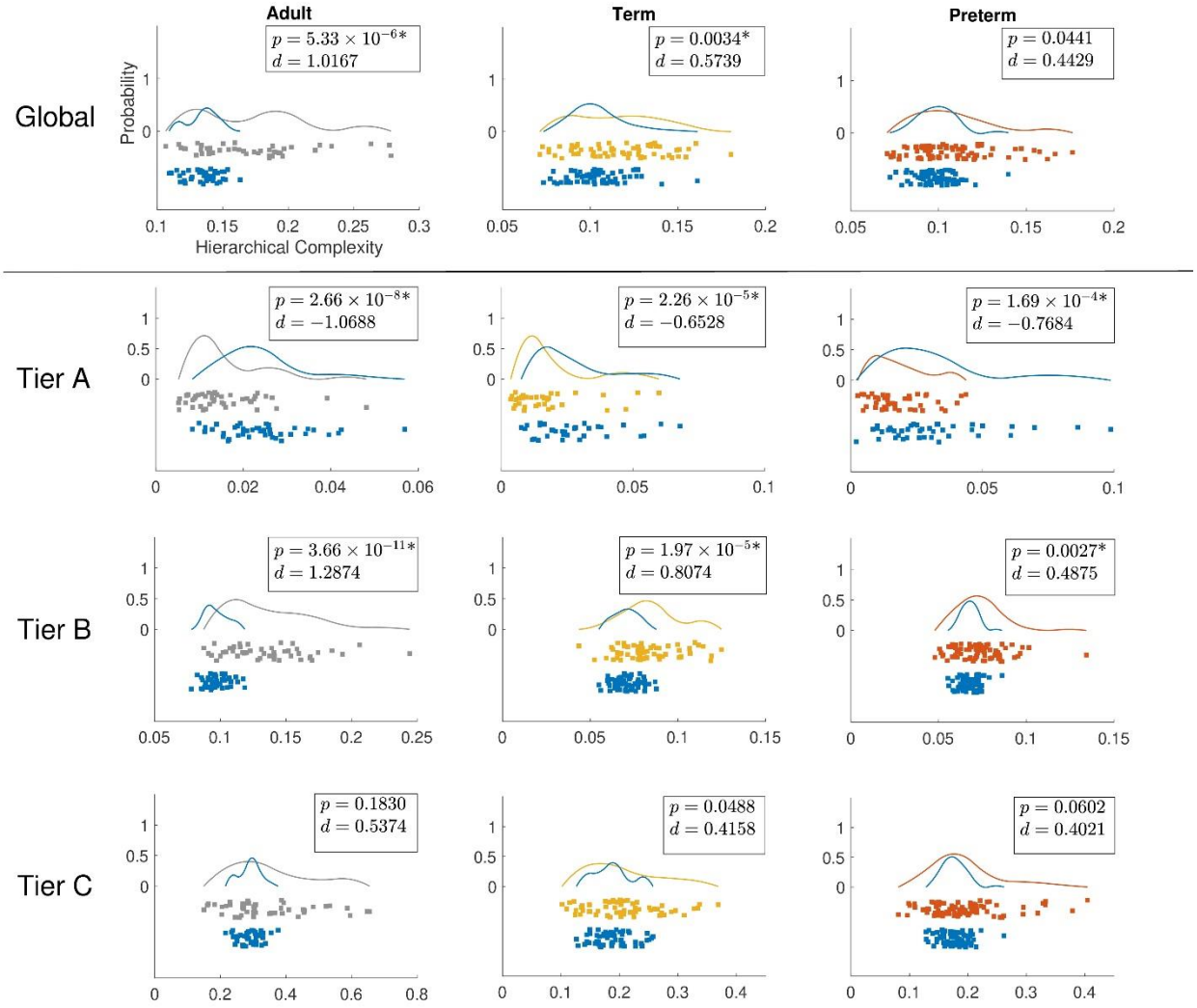

Figure 3: Distributions of HC globally (top) and for the different tiers of the three populations. Grey, yellow and orange colours represent values for adults, term born and preterm born neonates, respectively, while blue represents the values of the HC for the corresponding configuration models. Wilcoxon rank sum p-values and Cohen's d values are shown top right of each plot. Axes as in bottom right plot.

Discussion and conclusions:

The HC is already present at birth, but still needs to develop to reach the full level of complexity of the adult brain. Preterm babies have different values compared to term babies, in fact the values are not different from a random network. Tier 3 could be discerned as the main cause of the global effect between term and preterm. Interestingly, Tier A shows lower HC than a random network, indicating that the high levels of hierarchy present a structured organization. These findings are in agreement with intuitive notions of natural and human hierarchies: order may be necessary at the top to create structural stability, and this order at top level is resilient to prematurity. All together is consistent with the hypothesis that term born babies have a greater maturation than preterm born babies, with topological properties going in the direction of the properties displayed by the adult connectomes.

References:

1 M. P. Van Den Heuvel, K. J. Kersbergen, M. A. De Reus, K. Keunen, et al., The neonatal connectome during preterm brain development, Cerebral Cortex 25 (2015) 3000–3013

2 D. Batalle, E. J. Hughes, H. Zhang, J.-D. Tournier, N. Tusor, others., Early development of structural networks and the impact of prematurity on brain connectivity, NeuroImage 149 (2017) 379–392.

3 G. Ball, P. Aljabar, S. Zebari, N. Tusor, T. Arichi, N. Merchant, E. C. Robinson, E. Ogundipe, D. Rueckert, A. D. Edwards, S. J. Counsell, Rich-club organization of the newborn human brain, Proceedings of the National Academy of Sciences 111 (2014) 7456–7461.

4 K. Smith, M. Bastin, S. Cox, M. Valdes-Hernandez, S. Wiseman, J. Escudero, C. Sudlow, Hierarchical complexity of the adult human structural connectome, Neuroimage 191 (2019) 205–215.

5 K. Smith, On neighbourhood degree sequences of complex networks, Scientific Reports 9 (2019) 8340.

6 J. Veraart, D. S. Novikov, D. Christiaens, B. Ades-aron, J. Sijbers, E. Fieremans, Denoising of diffusion MRI using random matrix theory, NeuroImage 142 (2016b) 394–406

7 J. L. Andersson, S. N. Sotiropoulos, An integrated approach to correction for off-resonance effects and subject movement in diffusion MR imaging, NeuroImage 125 (2016) 1063–107

8 J. L. Andersson, M. S. Graham, E. Zsoldos, S. N. Sotiropoulos, Incorporating outlier detection and replacement into a non-parametric framework for movement and distortion correction of diffusion MR images, NeuroImage 141 (2016) 556–572.

9 J. L. Andersson, M. S. Graham, I. Drobnjak, H. Zhang, N. Filippini, M. Bastiani, Towards a comprehensive framework for movement and distortion correction of diffusion MR images: Within volume movement, NeuroImage 152 (2017) 450–466.

10 N. J. Tustison, B. B. Avants, P. A. Cook, Y. Zheng, A. Egan, P. A. Yushkevich, J. C. Gee, N4ITK: Improved N3 bias correction, IEEE Transactions on Medical Imaging 29 (2010) 1310–1320.

11 A. Makropoulos, E. C. Robinson, A. Schuh, R. Wright, S. Fitzgibbon, et al., The developing human connectome project: A minimal processing pipeline for neonatal cortical surface reconstruction, NeuroImage 173 (2018) 88–112

12 B. Alexander, A. L. Murray, W. Y. Loh, L. G. Matthews, C. Adamson, R. Beare, J. Chen, C. E. Kelly, S. Rees, S. K. Warfield, P. J. Anderson, L. W. Doyle, A. J. Spittle, J. L. Cheong, M. L. Seal, D. K. Thompson, A new neonatal cortical and subcortical brain atlas: the melbourne children's regional infant brain (m-crib) atlas, NeuroImage 147 (2017) 841 – 851.

13 B. Avants, C. Epstein, M. Grossman, J. Gee, Symmetric diffeomorphic image registration with cross-correlation: Evaluating automated labeling of elderly and neurodegenerative brain, Medical Image Analysis 12 (2008) 26 – 41. Special Issue on The Third International Workshop on Biomedical Image Registration WBIR 2006.

14 H. Wang, J. W. Suh, S. R. Das, J. B. Pluta, C. Craige, P. A. Yushkevich, Multi-atlas segmentation with joint label fusion, IEEE Transactions on Pattern Analysis and Machine Intelligence 35 (2013) 611–623

15 M. F. Glasser, S. N. Sotiropoulos, J. A. Wilson, T. S. Coalson, B. Fischl, J. L. Andersson, J. Xu, S. Jbabdi, M. Webster, J. R. Polimeni, D. C. V. Essen, M. Jenkinson, The minimal preprocessing pipelines for the human connectome project, NeuroImage 80 (2013) 105 – 124. Mapping the Connectome.

16 R. S. Desikan, F. Sgonne, B. Fischl, B. T. Quinn, B. C. Dickerson, D. Blacker, R. L. Buckner, A. M. Dale, R. P. Maguire, B. T. Hyman, M. S. Albert, R. J. Killiany, An automated labeling system for subdividing the human cerebral cortex on mri scans into gyral based regions of interest, NeuroImage 31 (2006) 968 – 980

17 J.-D. Tournier, F. Calamante, A. Connelly, Robust determination of the fibre orientation distribution in diffusion mri: Non-negativity constrained super-resolved spherical deconvolution, NeuroImage 35 (2007) 1459 – 1472.

18 T. Dhollander, D. Raffelt, A. Connelly., Unsupervised 3-tissue response function estimation from single-shell or multi-shell diffusion mr data without a co-registered t1 image., in: ISMRM Workshop on Breaking the Barriers of Diffusion MRI.

19 B. Jeurissen, J.-D. Tournier, T. Dhollander, A. Connelly, J. Sijbers, Multi-tissue constrained spherical deconvolution for improved analysis of multi-shell diffusion mri data, NeuroImage 103 (2014) 411 – 426

20 R. E. Smith, J.-D. Tournier, F. Calamante, A. Connelly, Anatomically-constrained tractography: Improved diffusion mri streamlines tractography through effective use of anatomical information, NeuroImage 62 (2012) 1924 – 1938.

21 R. E. Smith, J.-D. Tournier, F. Calamante, A. Connelly, Sift2: Enabling dense quantitative assessment of brain white matter connectivity using streamlines tractography, NeuroImage 119 (2015) 338 – 351.

22 K. Smith, J. Escudero, The complex hierarchical topology of eeg functional connectivity, Journal of Neuroscience Methods 276 (2017) 1–12.

23 S. Maslov, K. Sneppen, Specificity and stability in topology of protein networks, Science 910 (2002) LP–913.